Cell, Vol. 121, 479–492, May 6, 2005, Copyright ©2005 by Elsevier Inc. DOI 10.1016/j.cell.2005.02.012

Mosaic Analysis with Double Markers in Mice

Resource

Hui Zong,[1] J. Sebastian Espinosa,[1,2] Helen Hong Su,[1] Mandar D. Muzumdar,[1,3] and Liqun Luo[1,2,*]
[1]Department of Biological Sciences
[2]Neurosciences Program
[3]School of Medicine
Stanford University
Stanford, California 94305

Summary

We describe a method termed MADM (mosaic analysis with double markers) in mice that allows simultaneous labeling and gene knockout in clones of somatic cells or isolated single cells in vivo. Two reciprocally chimeric genes, each containing the N terminus of one marker and the C terminus of the other marker interrupted by a loxP-containing intron, are knocked in at identical locations on homologous chromosomes. Functional expression of markers requires Cre-mediated interchromosomal recombination. MADM reveals that interchromosomal recombination can be induced efficiently in vivo in both mitotic and postmitotic cells in all tissues examined. It can be used to create conditional knockouts in small populations of labeled cells, to determine cell lineage, and to trace neuronal connections. To illustrate the utility of MADM, we show that cerebellar granule cell progenitors are fated at an early stage to produce granule cells with axonal projections limited to specific sublayers of the cerebellar cortex.

Introduction

Genetic mosaics, in which somatic cells of different genotypes reside in the same animal, have been widely used to study biological processes in multicellular organisms. By knocking out a candidate gene of interest in a defined population of cells at a desirable time, one can study gene function in biological processes of interest while bypassing possible requirements for the gene in other tissues or at earlier developmental stages. One can also analyze the cell autonomy of gene function and create animal models of human diseases that result from somatic mutations. For example, conditional knockouts of tumor suppressor genes can serve as models for human cancers caused by loss of heterozygosity (Knudson, 1971).

Several methods have been employed to create genetically mosaic animals (Zugates and Lee, 2004). Genetic mosaics in mice are usually created via a conditional knockout procedure utilizing Cre-loxP mediated *intrachromosomal* recombination. In this strategy, two loxP sites are inserted flanking an essential part of a candidate gene (creating a floxed allele) by homologous recombination in embryonic stem (ES) cells. Cre recombinase, supplied as a transgene under the control of specific promoters, dictates the temporal and spatial specificity of the loss of the candidate gene by intrachromosomal excision in animals homozygous for a floxed allele or heterozygous for a floxed and a null allele (Gu et al., 1994; Lewandoski, 2001).

In *Drosophila*, a different strategy utilizing *interchromosomal* recombination prior to cell division (mitotic recombination) has been widely used to create genetically mosaic animals. This strategy employs a yeast site-specific FLP recombinase that mediates high frequency recombination at homologous chromosomal loci bearing the FLP recognition target (FRT; Golic and Lindquist, 1989). FLP is supplied as a transgene driven by specific promoters to direct mitotic recombination at the desired time and tissue. By placing FRT sites at the bases of major chromosomal arms, FLP-FRT-mediated mitotic recombination allows the vast majority of *Drosophila* genes to be subjected to mosaic analysis and permits forward genetic screens to be conducted in mosaic animals (Xu and Rubin, 1993). This mitotic recombination-based mosaic analysis has advantages over the aforementioned conditional knockout method in mice. It can be used with spontaneously generated or chemically induced mutations and does not involve engineering floxed alleles on a gene-by-gene basis.

To facilitate genetic mosaic analysis, it is essential to mark cells of different genotypes in mosaic animals. In mice, existing methods for simultaneous conditional gene knockout and labeling include using an independent Cre reporter, inserting a marker gene directly downstream of a floxed allele, or juxtaposing a reporter to the endogenous promoter by Cre-induced inversion (Lewandoski, 2001, Schnütgen et al., 2003). The first method cannot guarantee 100% coupling of knockout and labeling, especially for gene knockout in small populations of cells. The latter two methods allow 100% coupling but rely on the endogenous promoter to drive marker expression, which may be turned off or too weak at the time of analysis. In *Drosophila*, mosaic marking was originally accomplished using a negative labeling system in which homozygous mutant cells lose a marker gene and become the only unlabeled cells in genetically mosaic animals (Xu and Rubin, 1993). However, small clones of unlabeled homozygous mutant cells can be difficult to identify amid a large population of labeled cells, and the morphology of these mutant cells cannot be studied. To circumvent these limitations, we developed the MARCM system (mosaic analysis with a repressible cell marker) to selectively label homozygous mutant cells after FLP-FRT-induced mitotic recombination (Lee and Luo, 1999), offering high-resolution phenotypic analysis of gene function in complex processes ranging from neuronal morphogenesis (e.g., Lee et al., 2001; Grueber et al., 2002) to tumor metastasis (Pagliarini and Xu, 2003). Because MARCM allows labeling of a single cell or a group of cells that share a common progenitor, it has become a powerful tool for analyzing the relationship between neuronal lineage and wiring pattern (Lee et al., 1999; Jefferis et al.,

*Correspondence: lluo@stanford.edu

2001) and between inputs and outputs of neurons within a neural circuit (Marin et al., 2002).

In principle, the Cre-loxP recombination system could be used to induce mitotic recombination in mouse somatic cells in a similar fashion to FLP-FRT-mediated mitotic recombination in *Drosophila*. However, *Drosophila* is unique among model organisms in that homologous chromosomes pair in somatic cells, permitting a high rate of mitotic recombination (Metz, 1916). It remained uncertain whether the frequency of interchromosomal recombination would be sufficient for use in mosaic analysis in mice. Previous studies in mouse ES cells have reported that the frequency of Cre-loxP-mediated recombination, as assayed by formation of drug-resistant colonies following transient Cre transfection, was on the order of 10^{-7} to 10^{-4} between nonhomologous chromosomes (Ramirez-Solis et al., 1995; Smith et al., 1995; Van Deursen et al., 1995; Zheng et al., 2000); recombination between the same loci on homologous chromosomes had an increased efficiency of 10^{-4} to $\sim 5 \times 10^{-2}$ depending on the chromosomal locus tested (Liu et al., 2002; Koike et al., 2002). Constitutive Cre expression in ES cells further increased the rate of recombination (Liu et al., 2002). We hypothesized that if Cre-loxP-mediated interchromosomal recombination occurs in somatic cells at rates similar to ES cells, it can be used to create genetic mosaics, provided that one can develop a sensitive marking system to identify recombination events.

Here, we describe a system utilizing Cre-loxP to generate and mark recombination events between homologous chromosomes in somatic cells of mice. We show that interchromosomal recombination can be induced efficiently in both mitotic and postmitotic cells as a consequence of Cre expression. We discuss the potential utility of this system in conditional gene knockout, lineage analysis, and neural circuit tracing. As an example, we show that cerebellar granule cell progenitors are fated at an early stage to produce granule cells that project axons to specific sublayers in the molecular layer of the cerebellar cortex.

Results

The MADM Strategy

MADM makes use of Cre-loxP-dependent interchromosomal mitotic recombination to generate uniquely labeled homozygous mutant cells in an otherwise heterozygous background in mice. Figure 1 illustrates the MADM design. Two reciprocally chimeric marker genes are separately targeted by homologous recombination to identical loci on homologous chromosomes; the resultant mice are crossed to each other to make transheterozygotes. Each chimeric gene consists of part of the coding sequences of green fluorescent protein (GFP) and red fluorescent protein (Dsred2; hereafter referred to as RFP; Figure 1A; these chimeric genes are referred to as GR and RG hereafter). The N- and C-terminals of each chimeric gene are separated by an intron containing a single loxP site. While this pair of loxP sites serves as a target for Cre-mediated interchromosomal recombination, protein expression is unaffected since the loxP sites are removed by RNA splicing. In the absence of recombination, these chimeric genes do not produce functional proteins because their coding sequences are interrupted by the intron in different reading frames.

After DNA replication in dividing cells (at the G2 phase), Cre enzyme introduced as a separate transgene can induce recombination between loxP sites, restoring functional GFP and RFP expression cassettes. During the subsequent mitosis, two types of chromosomal segregations are possible. X segregation (two recombinant sister chromatids segregate into different daughter cells) produces two daughter cells, each capable of expressing one of the two functional fluorescent proteins (red or green). Z segregation (two recombinant sister chromatids segregate into the same daughter cell) generates one daughter cell that resembles the parental cell (colorless) and a second daughter cell expressing both fluorescent proteins (double colored) (Figure 1A). Recombination can also occur in the G1 phase of the cell cycle or in postmitotic cells (G0). In both cases, functional GFP and RFP are restored simultaneously, resulting in double-colored cells (Figure 1B).

If one chromosome contains a mutation of interest distal to the GR knockin site (the homologous chromosome contains only RG), the animal will be heterozygous for the mutation. However, G2 recombination followed by X segregation (referred to hereafter as a G2-X event) generates green daughter cells homozygous for the mutation and red siblings homozygous for the wild-type allele, creating labeled genetic mosaics (Figure 1A, left branch). G2-Z, G1, or G0 events do not alter the heterozygous genotype and do not result in the generation of single-labeled cells (Figure 1A, right branch; Figure 1B). Thus, recombination/segregation events that alter genotypes (G2-X) can be unambiguously distinguished from other recombination events that do not alter genotypes. Only homozygous cells are singly labeled. Furthermore, homozygous mutant and wild-type cells are distinguished by which single marker they express.

Generation and Testing of the Targeting Constructs

We generated three targeting constructs, GG, GR, and RG (Figure 2A). Each construct contains the same expression cassette consisting of a CMV β-actin enhancer-promoter (pCA; Okada et al., 1999; Niwa et al., 1991) and the SV40 T antigen poly(A) signal that allows for ubiquitous and high-level expression of marker genes. GR and RG were built according to the MADM strategy (Figure 1A). GG, in which N-GFP and C-GFP in the same reading frame are separated by the same loxP-containing β-globin intron, serves as a positive control for promoter strength, splicing efficiency, and the influence of chromosomal locus on transgene expression. We also constructed an RR construct equivalent to GG for in vitro testing.

Experiments were conducted to confirm marker expression along the construction of the final targeting vector (Figure 2A). The splicing efficiency of the loxP-containing intron was confirmed by Western blot analysis following COS cell transfection of the GG and RR constructs—they express proteins at the same level as

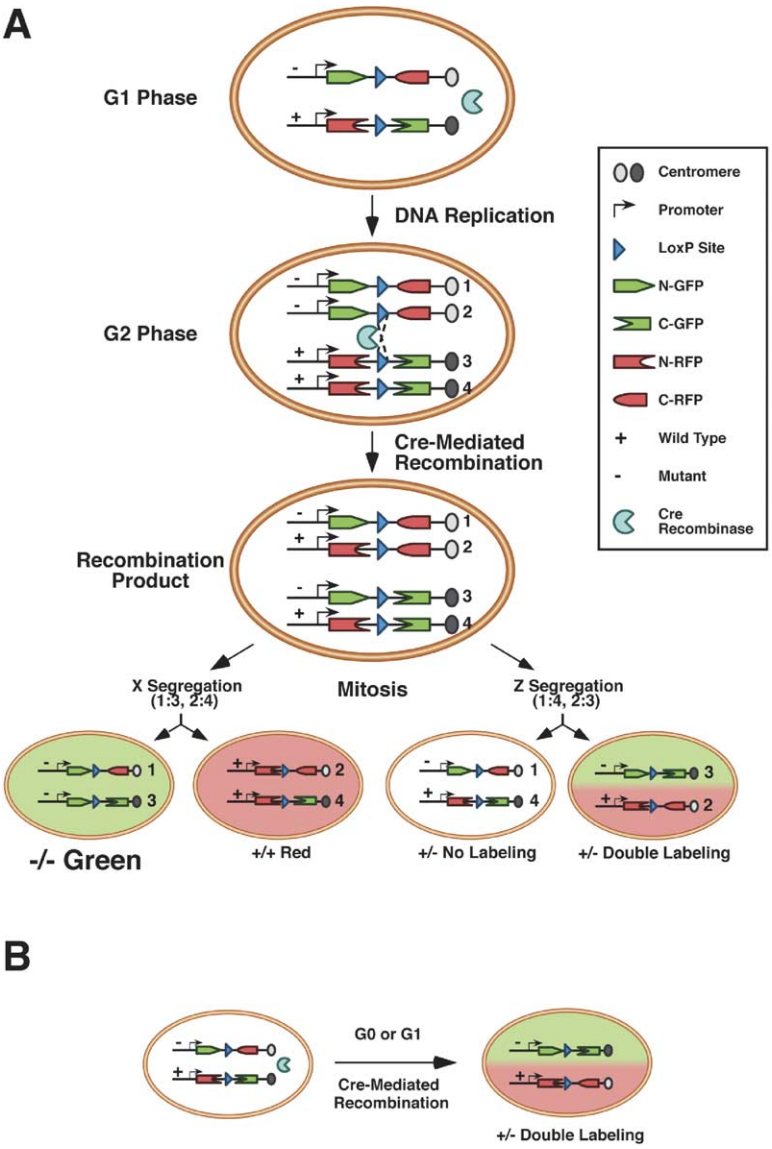

Figure 1. Schematic of the MADM Strategy

(A) G2 recombination followed by X segregation generates singly labeled cells that alter genotype if the original cell is heterozygous for a mutation of interest. G2 recombination followed by Z segregation generates either colorless or double-colored cells without altering genotype.

(B) Recombination occurring in G1 or postmitotic cells (G0) generates double-colored cells without altering genotype.

intronless constructs (data not shown). The expression level was also tested in neurons by biolistic transfection of rat hippocampal slices (Nakayama et al., 2000). GFP labeled axons and the entire dendritic trees including dendritic spines (Figure 2B, left, inset). Since RFP fluorescence is markedly weaker compared with GFP (data not shown), a MYC tag was added to the C terminus of RFP to ensure detection (Figure 2B, right). Functional restoration of GFP/RFP in the chimeric constructs (lacking the *Neo*^{r} cassette) was verified by cotransfecting GFP/RFP chimeras and a Cre-expressing construct into hippocampal slices. Double-colored cells were only generated when all three constructs were cotransfected (Figure 2C), indicating that Cre could catalyze interplasmid recombination that reconstitutes GFP and RFP.

Having validated the chimeric marker approach in vitro, a loxP-neomycin resistance (*Neo*^{r}) gene was inserted into the intron of GG, GR, and RG for positive selection of homologous recombination events in ES cells. These constructs were knocked in at the *ROSA26* locus (Soriano, 1999) on the long arm of mouse chromosome 6 to test the MADM strategy in vivo. *ROSA26* was chosen because of the following advantages: First, *ROSA26* allows ubiquitous expression of the inserted gene (Zambrowicz et al., 1997). Even though our chimeric genes contain their own ubiquitously active promoter, targeting at the *ROSA26* locus alleviates concerns about silencing effects of local chromatin structure. Second, mice homozygous for *ROSA26* targeted insertions do not exhibit detectable phenotypes (Soriano, 1999). This is critical because MADM requires knockin cassettes at the locus for both homologous chromosomes.

Cre-Dependent Generation of Labeled Cells In Vivo

We generated GG, GR, and RG knockin mice using standard ES cell-based homologous recombination. As

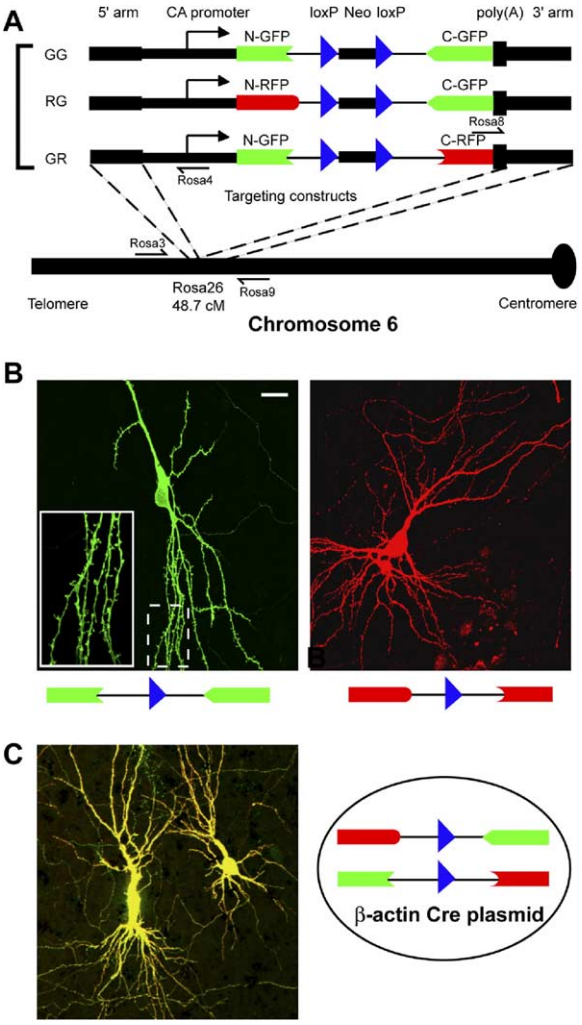

Figure 2. Generation and Testing of MADM-Targeting Constructs

(A) Schematic of final targeting constructs.

(B) Biolistic transfection of test constructs in brain slices shows that GFP and RFP-MYC fill all neuronal processes including dendritic spines (inset).

(C) Cotransfection of chimeric constructs with Cre restores GFP and RFP-MYC expression.

MYC staining was used in (B) and (C) for detection of RFP-MYC. Scale, 20 μm.

expected in the GG strain, GFP is ubiquitously produced from embryo to adult in the brain (Figure 3A) and all other tissues examined (data not shown). Nearly 100% of cells dissociated from the brain and spleen were GFP positive by fluorescence microscopy or by FACS analysis (data not shown). This confirmed ubiquitous expression of the artificially assembled expression cassette at the *ROSA26* locus.

As predicted, mice heterozygous for GR and RG (GR/RG) do not have colored cells in the absence of Cre-mediated recombination. This was confirmed by examining >20 GR/RG mouse brains through serial sagittal sections without observing a single GFP or RFP-MYC labeled cell (Figure 3B) and by FACS analysis of dissociated cells from these mice (data not shown). When various Cre transgenes were separately introduced to create mice containing GR, RG, and Cre (GR/RG;Cre/+), we observed cells labeled with GFP, RFP-MYC,or both in patterns predicted by Cre expression (Table 1).

For example, nestin-Cre generates MADM-labeled cells throughout the brain (Figure 3C), consistent with its expression in all neural precursors (Lendahl et al., 1990). In contrast, labeled cells in GR/RG;Foxg1-Cre/+ mice are highly enriched in the forebrain and granule cells of the cerebellum but not in the brain stem (Figure 3D), consistent with the previously reported expression pattern of Foxg1-Cre (Hebert and McConnell, 2000). We also observed a nasal to temporal gradient of labeled cells in the retina (Figure 3E) that followed the Foxg1-Cre expression pattern (Hebert and McConnell, 2000).

Cre transgenes driven by promoters of ubiquitously expressed genes, such as hprt-Cre (Tang et al., 2002) or actin-Cre (Lewandoski et al., 1997), permit cell labeling outside the nervous system (Table 1; Figure 4). For example, hprt-Cre allows the labeling of cells in the liver (Figure 4A), kidney (Figure 4B), heart (Figure 4C), spleen (Figure 4D), and all other tissues examined (data not shown). Actin-Cre generates labeled cells in the epidermis (Figure 4E) as well as in the brain (see below), while keratin5-Cre (K5-Cre), which is expressed only in keratinocyte precursors (Brakebusch et al., 2000), generates labeled cells only in the epidermis (Figure 4F) but not in the brain (data not shown).

Visualization of Both Markers

One distinctive feature of MADM is the ability to distinguish between different recombination/segregation types using the double-marker system (Figure 1). We found that GFP can be visualized by fluorescence in live or fixed samples, whereas RFP fluorescence cannot. Since RFP was tagged with C-terminal MYC, anti-MYC immunofluorescence allowed simultaneous visualization of both markers in neurons, glia, and other nonneural tissues in fixed samples during development and in the adult (Figures 3F–H and 4; data not shown). Double-labeled cells (e.g., yellow cells in Figures 3F, 3H, and 4Aa–4Dc) are readily distinguishable from single-green and single-red cells, allowing for the distinction of G2-X events from those of G0, G1, or G2-Z events. In many cases, particularly in nonneural tissues where cell migration is limited, single-green and single-red cells form clusters adjacent to each other ("twin spots;" e.g., Figures 3G, 4Ac, 4Bc, 4Cc, 4Eb, and 4Fb), strongly suggesting that they are progeny of siblings derived from single G2-X events.

Labeling Efficiency of MADM

We find that a given Cre line not only dictates the spatial pattern of the MADM recombination events but also the frequency and type of labeled cells (Table 1). For example, a much higher labeling efficiency is achieved with K5-Cre compared with actin-Cre in the epidermis (Figure 4E versus Figure 4F). Likewise, hprt-Cre generates many more MADM-labeled cells than actin-Cre in the brain and elsewhere (Table 1).

The efficiency of G2-X events (single-labeled cells) relative to other events (double-labeled cells) also varied according to the Cre lines used. As expected, lines

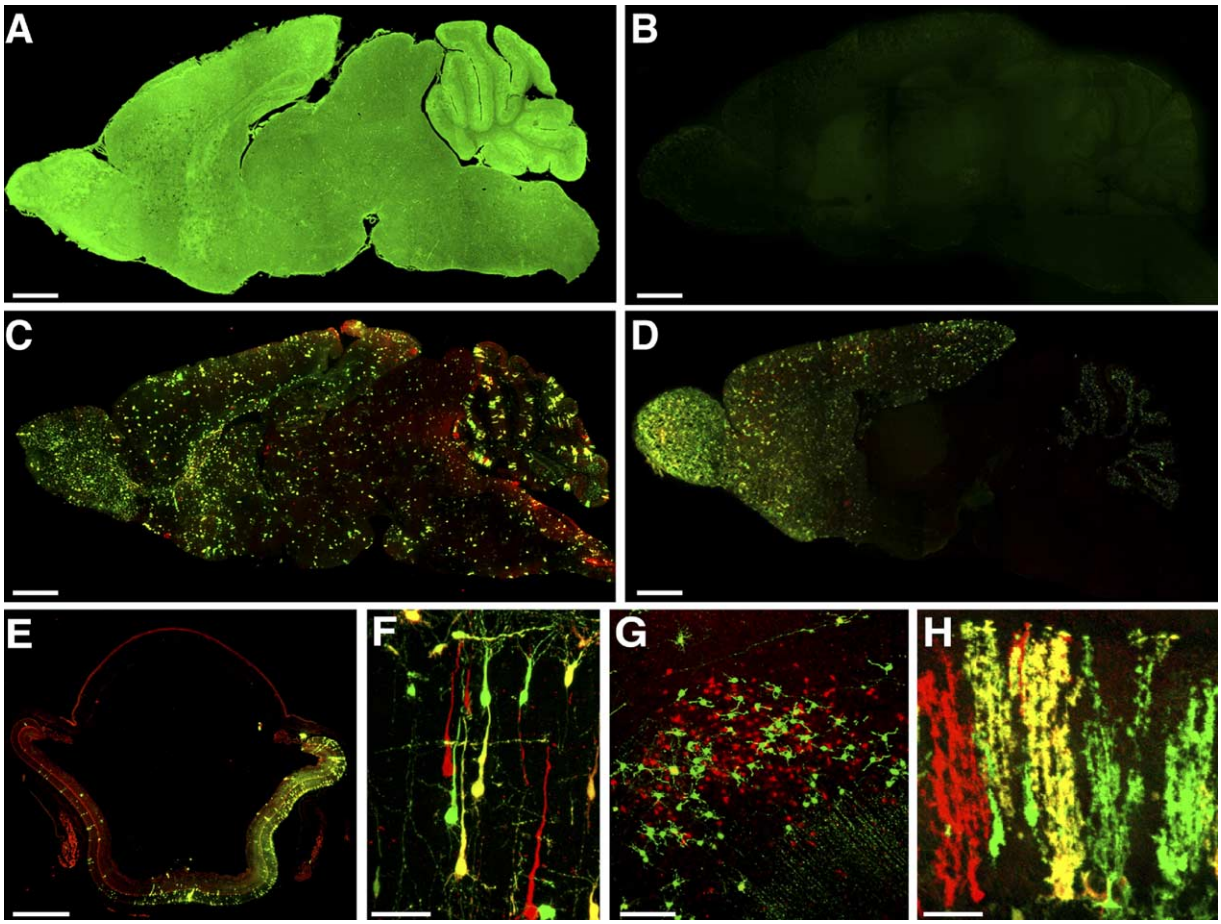

Figure 3. Cre-Dependent Generation of Labeled Cells in the Nervous System

(A) Sagittal section of an adult GG mouse brain, showing uniform expression of GFP.

(B) Sagittal section of an adult GR/RG brain, showing lack of expression of GFP or RFP-MYC when imaged under similar conditions as in (A).

(C) Sagittal section of a P21 GR/RG;nestin-Cre/+ brain, showing labeled cells scattered throughout the brain.

(D) Sagittal section of a P21 GR/RG;Foxg1-Cre/+ brain, showing labeled cells enriched in the forebrain and the cerebellum but not in the brain stem.

(E) Cross-section of a GR/RG;Foxg1-Cre/+ retina, showing a nasal-temporal gradient of labeled cells. Nasal to the right.

(F) High magnification of the cerebral cortex of a P2 GR/RG;nestin-Cre/+ mouse showing distinction of green, red, and double-colored neurons.

(G) A cluster of cerebellar granule cells labeled in green or red but not both, from a GR/RG;actin-Cre/+ adult mouse. Based on the very low frequency of single-colored cells for this genotype, these cells are most likely to be the progeny of a single G2-X event. Superimposed on this G2-X event, there are also a few isolated yellow granule cells at a similar density in this and other fields, presumably caused by independent recombination events. Note that neuronal processes are more efficiently labeled with green than red.

(H) Labeled Bergmann glia in cerebellar cortex of a P21 GR/RG;nestin-Cre/+ mouse showing clear distinction of green, red, and double-colored cells.

Scale: (A)–(D) 1 mm; (E) 500 μm; (F) and (H) 50 μm; (G) 100 μm.

of mice where Cre is transiently expressed in dividing cells have a higher frequency of G2-X events, as in the case of nestin-Cre or K5-Cre (Figures 3C, 3F, 3H, and 4F). For ubiquitous Cre lines, the proportion of double-colored cells increases with age, as would be predicted if postmitotic recombination happened throughout a cell's life.

To test the relationship between labeling frequency and Cre dose and to confirm postmitotic recombination, we devised a quantitative assay that evaluates the frequency of labeled cerebellar granule cells. Each granule cell gives rise to a single axon that runs along the molecular layer of the cerebellar cortex in parallel to axons of other granule cells (forming "parallel fibers"). Near the midline, these parallel fibers run along the medial-lateral axis and each axon appears as a dot in sagittal sections (Figure 5A). Thus, the number of dots in a defined area of the molecular layer can be used to assess the labeling frequency of granule cells. We found that doubling the dose of actin-Cre caused an approximate 2-fold increase in labeling frequency (Figure 5B). In addition, the density of labeled parallel fibers increases significantly from postnatal day 21 (P21) to P42 (Figure 5B). Since granule cell neurogenesis ceases at P21, newly labeled cells after P21 should be products of postmitotic recombination.

Table 1. Labeling Efficiency by MADM with Different Cre Lines

Cre Line	Expression Pattern	Labeling Efficiency	References
β-actin	Ubiquitous	++ (single copy) +++ (double copy)	Lewandoski et al., 1997
K5	Epidermal	+++++	Brakebusch et al., 2000
Hprt	Ubiquitous	+++++	Tang et al., 2002
Foxg1	Forebrain	+++++	Hebert and McConnell, 2000
nestin-Cre9.5	Neuronal and glial precursor	++++	Tronche et al., 1999
nestin-Cre8.5	Same as above	++++	Petersen et al., 2002
Wnt1	Midbrain and cerebellum	+++	Danielian et al., 1998
En1	Midbrain and cerebellum	+++++	Kimmel et al., 2000
β-actin-CreER	Ubiquitous, inducible	+	Guo et al., 2002

+ Few labeled cells per brain.
++ 0.001–0.01% cells are labeled (based on the observation that 100–1000 labeled cells/100 μm slice and a brain can be cut into ~100 slices. So 10^4–10^5 cells are labeled in each brain, which contains 10^8–10^9 cells. This leads to the estimation of 0.001–0.01%.).
+++ 0.01–0.1% cells are labeled (based on comparison to ++ brains).
++++ 0.1–1% cells are labeled (based on comparison to +++ and +++++ brains).
+++++ 2–5% cells are labeled (based on FACS analysis of Foxg1- and Hprt-Cre lines and comparison to other lines).
Note: These estimates correspond to the order of magnitude of total labeled cells. In most cases, single-labeled cells are a minority and the proportion to double-labeled cells decreases with age.

To assess labeling efficiency and the relative frequency of G2-X events in the developing brain, we dissociated cells from cortical caps of GR/RG;Foxg1-Cre/+ mice at P5. These cells were stained with anti-GFP and anti-MYC antibodies, and green, red, and double-labeled cells were counted with fluorescence

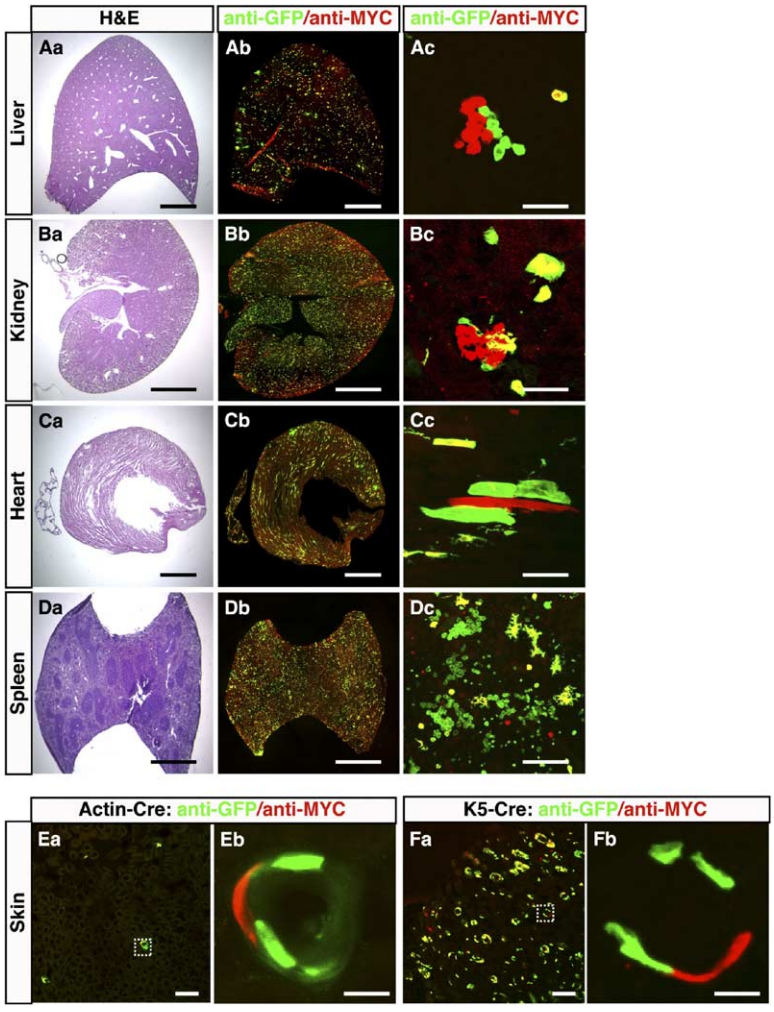

Figure 4. MADM-Labeled Cells in Nonneural Tissues

(A–D) Examples of MADM-labeled cells in the liver (A), kidney (B), heart (C), and spleen (D) in adult GR/RG;hprt-Cre/+ mice. (Aa)–(Da) are hematoxylin-eosin staining of adjacent sections of the low magnification fluorescence images shown in (Ab)–(Db). (Ac)–(Dc) are high magnification images of representative labeled cells and groups of cells in the respective tissues.

(E and F) Horizontal section of epidermis from a GR/RG;actin-Cre/+ mouse (Ea) or a GR/RG;K5-Cre/+ mouse (Fa) showing labeled epidermal cells of hair follicles. (Eb) and (Fb) are higher magnifications of (Ea) and (Fa) from the boxed regions.

Scale: (Aa)–(Da) and (Ab)–(Db), 2 mm; (Ac)–(Dc), 50 μm; (Ea) and (Fa), 100 μm; (Eb) and (Fb), 10 μm.

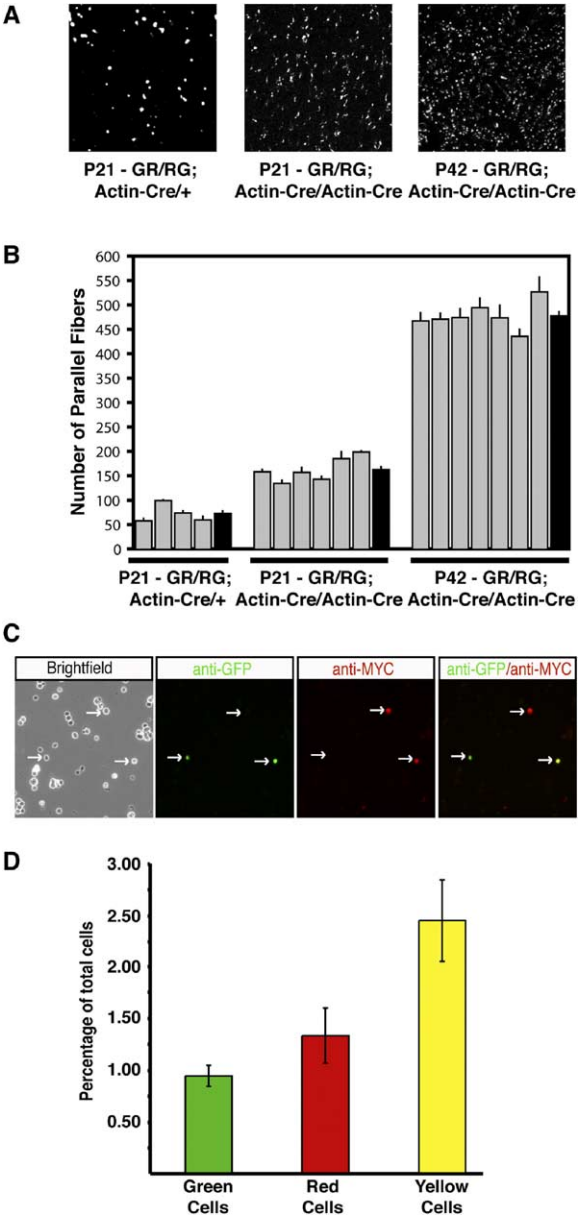

Figure 5. Quantification of MADM-Labeling Frequency

(A) Representative sagittal sections of the cerebellar molecular layer at the midline from mice of three different genotype/age combinations. Each dot is one labeled axon projecting perpendicular to the imaging plane, representing one MADM-labeled granule cell.

(B) Quantification of parallel fibers in a defined area of the molecular layer of cerebellar cortex. Each gray column represents average number (±SEM, n = 3) of labeled axons from a single mouse. Each black column represents the average of different mice of the same genotype.

(C) Representative images of dissociated cells from P5 cortical cap of GR/RG;Foxg1-Cre/+ mice labeled with GFP (green), MYC (red), or both. Also shown is a brightfield image of the same field.

(D) Quantification of the labeling frequency of (C). Error bars represent SEM. n = 4.

microscopy (Figure 5C). Green and red cells each consist of ~1% of total cells, while double-colored cells consist of ~2.5% of total cells (Figure 5D). We expect that this labeling frequency will permit analysis of gene knockouts in single cells of mosaic animals.

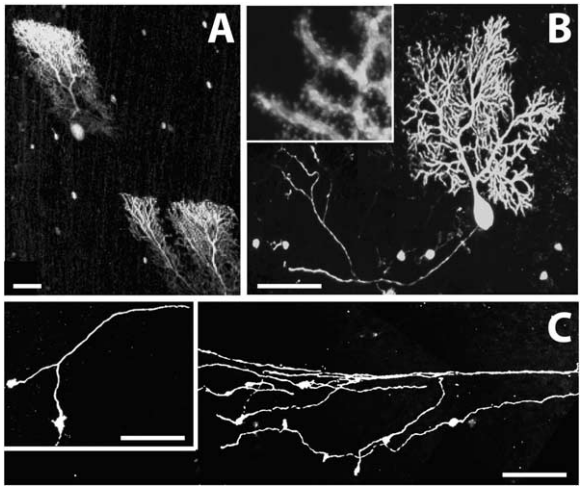

Figure 6. Resolution of Fine Structures of Neurons

(A) Confocal image of a live cerebellar slice from an adult mouse showing dendritic trees of two GFP-labeled Purkinje cells.

(B) Confocal image of a Purkinje cell from fixed tissue with high magnification inset showing dendritic spines.

(C) Confocal image of mossy fiber terminals in the internal granular layer of the cerebellar cortex. The left panel is a higher magnification of mossy fiber terminals from a different sample.

Genotypes: (A) and (B) GR/RG;actin-Cre/+; (C) GR/RG;actin-CreER/+ (TM administered at E13.5).

Scale: (A) and (B), 50 μm; (C), 100 μm; (C) inset, 50 μm.

Resolution of Fine Structures of Neurons

Analysis of neural circuit organization and development requires the ability to label and visualize axonal and dendritic projections of neurons in their entirety. Although previous approaches have achieved this purpose with multicopy transgene inserts (e.g., Feng et al., 2000; Gong et al., 2003), it was unclear whether a single copy gene from a knockin would be sufficient to label all neuronal processes. We found that the pCA promoter-driven single-copy GFP marker fulfills this purpose well in both live and fixed tissues. For example, GFP can label isolated Purkinje cells in live cerebellar slices (Figure 6A) or in fixed samples (Figure 6B). Dendritic trees, spines, and axonal projections are efficiently labeled (Figure 6B). Axon terminals of cerebellar mossy fibers, whose cell bodies reside millimeters away outside the cerebellum, can be visualized clearly in the internal granular layer of the cerebellar cortex (Figure 6C).

RFP-MYC allows the labeling of cell bodies, dendritic trees, proximal axons, and glial processes in fixed tissues using anti-MYC immunofluorescence (Figures 3F–3H). However, it does not label neuronal processes as well as GFP and does not label long-distance axons (see Figure 3G). Moreover, expression of single-copy RFP (Dsred2) is inadequate for live visualization. These limitations need to be overcome in future modifications of MADM.

Using MADM to Analyze Cerebellar Granule Cell Lineage and Axonal Projections

We are in the process of using MADM to perform conditional knockout experiments (see Discussion). To demonstrate other applications, we present here an example that uses MADM to illustrate an unexpected relationship between lineage and axonal projections of cerebellar granule cells.

The neural circuit in the cerebellum is one of the best characterized in the mammalian brain for both adult connectivity and its developmental origin. The adult cerebellar cortex is divided into several distinct layers (Figure 7B): the molecular layer (ML) consisting of granule cell axons forming parallel fibers that innervate Purkinje cell dendrites, the Purkinje cell layer (PC) made of Purkinje cell bodies, the internal granular layer (IGL) that houses cell bodies and dendrites of granule cells and axon terminals of the mossy fibers, and the white matter consisting of input axons to cerebellar cortex (mossy fibers and climbing fibers) and output axons from Purkinje cells. In the developing cerebellar cortex, granule cells are born from progenitors in the external granular layer (EGL) during the first 3 weeks of postnatal development. Postmitotic granule cells first extend axons parallel to the EGL and then descend their cell bodies into the IGL. Thus, the EGL is gradually replaced by the future ML. Previous studies have suggested that the first granule cells to exit the cell cycle and migrate into the IGL project axons to the deepest position of the ML and those that migrate subsequently occupy correspondingly more superficial positions (Cajal, 1911; Hatten and Heintz, 1995; Altman and Bayer, 1997).

To investigate the relationship between granule cell lineage and axon projection, we induced MADM clones in granule cell progenitors at embryonic stages using tamoxifen (TM) inducible actin-CreER (Guo et al., 2002) and examined the axonal projection patterns of granule cells derived from a common progenitor. In the absence of TM, CreER protein is in the cytoplasm and cannot catalyze DNA recombination. TM binding of CreER results in its nuclear translocation and activation (Feil et al., 1996). Previous experiments based on recombination efficiency and CreER subcellular localization indicated that Cre recombinase activity peaks within 6–24 hr and subsides 36 hr after TM administration (Hayashi and McMahon, 2002). Therefore, interchromosomal recombination and consequent labeling of granule cell progenitors occurs within approximately a day after TM administration.

We first administered TM to GR/RG;actin-CreER/+ mice at E17.5, a stage when most granule cell progenitors have occupied the EGL and are proliferating to give rise to more progenitors. We examined the progeny of these labeled clones at P21, a time when cerebellar cortex development is largely complete, including granule cell neurogenesis, axonogenesis, migration to the IGL, and dendrite differentiation. From 16 systematically sectioned half cerebella of 13 different mice, we found 26 distinct clusters of granule cells (e.g., Figure 7A). Several lines of evidence indicate that each cluster most likely represents progeny of a single-labeled granule cell progenitor at the time of TM administration. First, each cluster of granule cells forms a continuous domain along the anterior-posterior and medial-lateral axes with no labeled granule cells in between clusters, indicating limited dispersion. Second, the frequency of generating these clusters is low (1.6 per half cerebellum) under our experimental conditions. We estimate the probability of a single cluster actually consisting of two separate clonal lineages to be on the order of 5%, based on the relative sizes of the cerebellum and the clusters (see Experimental Procedures). Third, serial section of 7 GR/RG;actin-CreER/+ mice subjected to TM carrier (corn oil) injection at E17.5 did not reveal any labeled cells in the cerebellum or elsewhere in the brain, indicating that all labeled cells were caused by interchromosomal recombination induced by CreER shortly after TM injection. Therefore, we refer to these clusters of granule cells as clones. All 26 clones are double colored, indicating that they arose from either G2-Z, or more likely G1 recombination events in granule cell progenitors.

The distribution patterns of granule cell clones are consistent with previous clonal analysis of granule cells using retroviral infection in chick embryos (Ryder and Cepko, 1994). Collectively, they span every cerebellar folium along the anterior-posterior axis; each clone covers a wide span along the medial-lateral axis as measured by cell body position and parallel fiber extent (Figure S1A). Strikingly, for each clone, axonal projections appear to be confined to a specific sublayer within the ML, with some occupying superficial positions and others occupying middle or deep positions (Figure 7B).

To quantify this observation, we selected a representative region from a sagittal plane at the midpoint of each clone's mediolateral span and plotted the relative position of each parallel fiber in the ML. As evident from such a plot (Figure 7C, red dots), most clones restrict their axonal projections to less than half of the ML, with some as narrow as 10%. To measure the variability of axonal projections within the span of each clone, we compared these positional plots taken at the midpoint with those taken at the medial and lateral edge of each clone and compared the plots taken at the bank with those taken at the sulcus or gyrus of individual folia of the cerebellar cortex. We found consistent positional restriction of axonal projections within each granule cell clone (Figure S2).

We next examined MADM clones induced at E13.5, which label granule cell progenitors in the process of their migration from the rhombic lip to the EGL to cover the cerebellar surface. We found seven clones (from serial sections of 13 half cerebella) in different folia that span a wide range of medial-lateral positions (Figure S1B). Despite being induced at such an early stage, all seven clones show remarkable restriction of axonal projections to an extent similar to those of E17.5 induced clones. Axons within a clone are restricted to 20%–40% of the depth of the ML, but different clones occupy different sublayers from deepest to most superficial (Figures 7D and 7E).

Previous BrdU incorporation experiments have suggested a correlation between granule cell body position in the IGL and axon position in the ML: cell bodies of granule cells that differentiate earlier occupy deeper positions in the IGL and project axons to deeper parts of the ML (Altman and Bayer, 1997). We did not find a

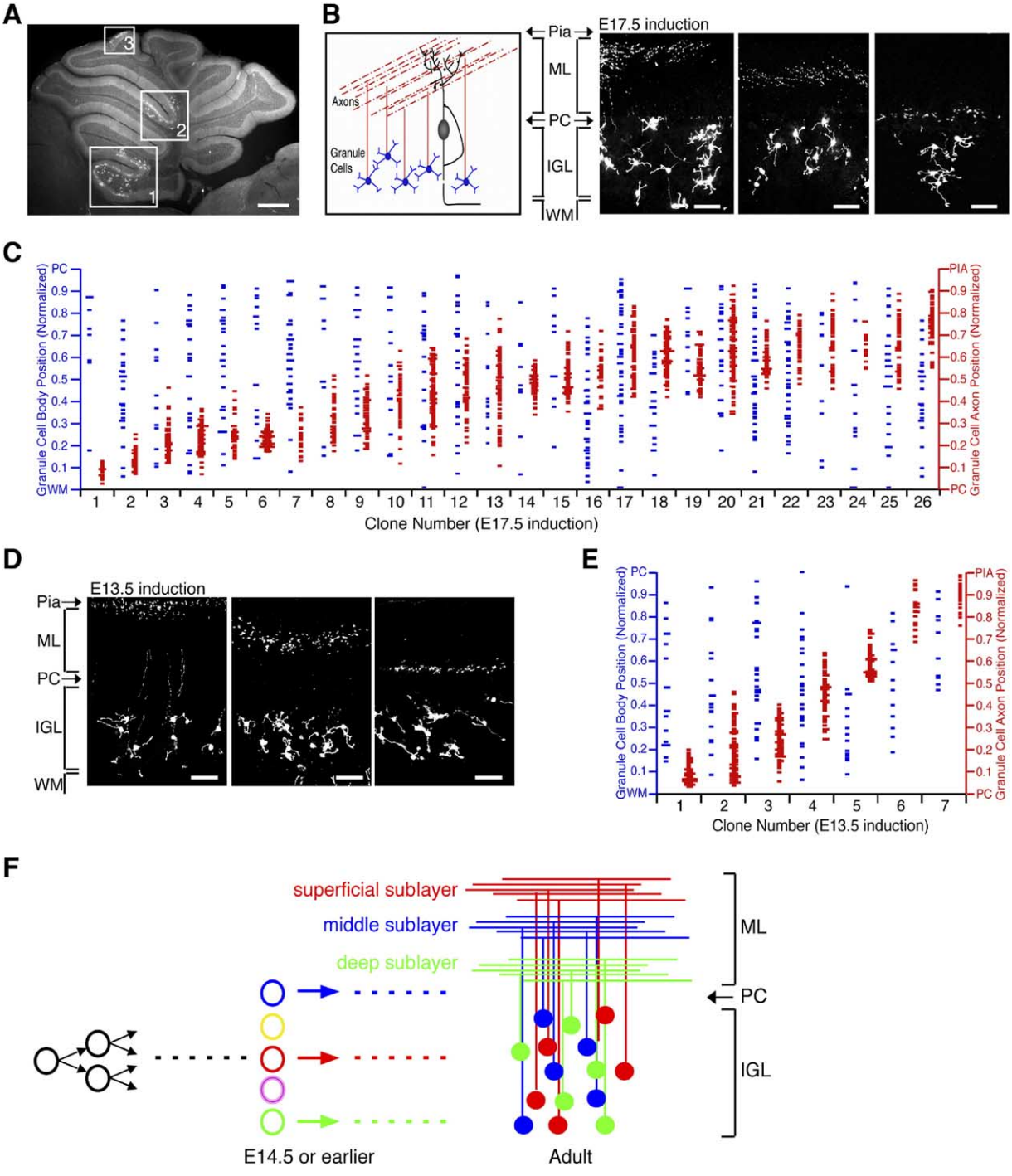

Figure 7. Analysis of Granule Cell Lineage and Axonal Projections Using MADM and CreER

(A) Sagittal section of a P21 cerebellum with three labeled granule cell clusters induced by 8 mg TM administration at E17.5. Scale, 1 mm.

(B and D) Confocal images of labeled granule cell clones induced by TM administration at E17.5 and E13.5, respectively. Each granule cell clone projects axons to a specific sublayer of the molecular layer. The left panel of (B) is a schematic drawing of the cerebellar cortex illustrating the organization of granule and Purkinje cells and their projections. ML, molecular layer; PC, Purkinje cell layer; IGL, internal granular layer; WM, white matter. Scale, 50 μm.

(C and E) Plots of granule cell body (blue) and axon (red) positions for granule cell clones induced at E17.5 (C) and E13.5 (E), respectively. Cell body position was measured as the distance from the IGL/WM border to individual cell bodies normalized by the span of the IGL. Axon position was measured from the PC to individual axons normalized by the span of ML.

(F) Schematic model illustrating that at an early developmental stage, granule cell progenitors are distinct with regard to the axonal projections of their progeny.

correlation between the cell body positions in the IGL and axon position in the ML; whereas axons from each clone are restricted to a specific sublayer of the ML, their corresponding cell body positions within each clone appear random in the IGL (Figures 7C and 7E).

In conclusion, these data indicate that prior to the completion of migration to EGL, individual cerebellar granule cell progenitors are fated to produce granule cells that project their axons to a specific sublayer of the ML (Figure 7F).

Discussion

Using Cre-loxP and a double-marker strategy, we show that interchromosomal recombination, both mitotic and postmitotic, can be induced efficiently in mammalian somatic cells in vivo. MADM can thus be used to label small populations of cells, to perform lineage analysis, to visualize wiring patterns in the nervous system, and to conditionally knock out genes in small populations of labeled cells with tight coupling of knockout and labeling. Moreover, MADM can be used for all the above purposes simultaneously. We discuss below potential applications of MADM compared with existing methods that achieve similar purposes.

Conditional Gene Knockout

Conditional knockouts based on Cre-loxP site-directed intrachromosomal recombination have been used to selectively knock out genes at particular developmental stages or in a subset of tissues (Lewandoski, 2001). It would be valuable to knock out genes in isolated cells and simultaneously visualize these mutant cells to examine phenotypes with high anatomical resolution. This has proven powerful in analyzing a wide range of biological processes in *Drosophila*. As mentioned in the Introduction, a general limitation of existing methods for marking mutant cells in conditional knockout is the difficulty to achieve strict coupling of knockout and labeling or to ensure strong marker expression.

MADM couples labeling and generation of homozygous cells through a single chromosomal exchange event, so there is little chance for ambiguity. Although experimental proof of tight coupling awaits a MADM-mediated knockout experiment in the future, we expect this to be the case as we have shown that the constitutive promoter (pCA) guarantees marker expression in 100% of cells in our GG mice. MADM also allows the labeling of homozygous wild-type siblings with a different color in the same animal, providing a built-in control for phenotypic analysis. Moreover, MADM does not require the gene of interest to be floxed; indeed, MADM can be used for conditional knockout of spontaneous or chemically induced mutations before they are cloned. These properties are of value, as there is an increasing effort to do extensive genetic screens in mice using chemical mutagens and to perform a systematic knockout mouse project without creating floxed alleles (Austin et al., 2004).

There are several limitations of MADM compared with conventional intrachromosomal recombination-based conditional knockouts. First, the efficiency of interchromosomal recombination is much less than the intrachromosomal recombination used for traditional conditional knockout. While this is advantageous for analyzing cell-autonomous gene function, it does not supersede traditional knockout if high recombination frequency is desirable (e.g., for analysis of nonautonomous phenotypes caused by loss of a secreted protein). Second, since gene knockout is coupled with mitosis in MADM, genes cannot be deleted at specific times in postmitotic cells. While this may not significantly affect developmental studies (and indeed might be a positive feature for certain developmental studies), it complicates analysis of gene function in adults if the gene of interest also plays a developmental role. This limitation might be remedied to some extent by temporally regulated transgene rescue (see below). Third, MADM-based gene knockouts rely on the availability of a pair of MADM knockins between the gene of interest and the centromere. At present, only genes located on mouse chromosome 6 distal to the *ROSA26* locus can be subjected to mosaic analysis using our current MADM mice. This limitation can be overcome by future effort to generate knockin cassettes for other chromosomes.

Labeling Small Populations of Neurons and Tracing Neural Circuits

Several methods exist for labeling small populations of neurons to trace neural circuits. These include (1) the traditional Golgi method, (2) dye filling, (3) Thy1-GFP transgenic mice, wherein chance insertions can create a mosaic expression pattern that labels isolated single neurons (Feng et al., 2000; De Paola et al., 2003), (4) transgenic mice using bacterial artificial chromosomes (BAC) to drive GFP expression using endogenous regulatory sequences, some of which result in GFP expression in small populations of neurons (Gong et al., 2003), and (5) CreER-based intrachromosomal recombination using low doses of TM in conjunction with a transgene reporter such as a loxP-stop-loxP marker (Badea et al., 2003; Buffelli et al., 2003). Dye filling is labor intensive (one cell at a time). The Golgi method can only label fixed tissue and is not reliable for long-distance axon labeling. Chance insertions of Thy1-GFP allow Golgi-like labeling of certain populations of neurons in fixed and live tissues, but the probability of targeting such labeling to a specific population of neurons is unpredictable. BAC-based transgenics are limited to the availability of endogenous genes that are expressed in a small population of neurons. MADM and CreER-based intrachromosomal recombination both have the potential to consistently label any type of neuron with controllable frequency by choosing specific Cre lines. Although genetically MADM is more complex, requiring three transgenes in the same mouse, once stable strains are established, it is as convenient. MADM has the added advantages of labeling clonally related cells and the potential to genetically manipulate labeled cells.

Lineage Tracing

Lineage tracing can be performed using transplantation, chimera, retrovirus infection, or recombination-based fate mapping (e.g., McConnell, 1988; Sanes, 1989; Bonnerot and Nicolas, 1993; Cepko et al., 1993; Hallonet and Le Douarin, 1993; Zinyk et al., 1998; Win-

gate and Hatten, 1999; Rodriguez and Dymecki, 2000; Zirlinger et al., 2002; Badea et al., 2003; Hashimoto and Mikoshiba, 2004). While some of these methods require embryonic manipulation, others are based on genetics. With the exception of retroviral infection, most methods provide little information about the birth date of the neurons whose lineages are to be traced.

It can be quite useful to decipher the developmental logic of neural circuit wiring if information regarding birth dates, lineage, and wiring pattern can be obtained in the same experiment (e.g., Jefferis et al., 2001). MADM-based clonal analysis and in particular G2-X events have several advantages in this regard. First, because G2-X mitotic recombination couples the generation of clones with mitosis, when used with CreER, MADM provides birth date information of single-cell clones or of the first progenitor of large clones. Second, G2-X events permit simultaneous labeling of two daughter cells (and all their descendents) from a single mitotic event with two different colors so that both lineages can be followed in the same animal to provide information about cell division pattern. This property is useful, for instance, to study stem cell behavior. Using temporally controllable Cre lines, one can activate Cre in the adult, and single-labeled cells must be generated through adult stem cells. Because of the double-marker strategy, one can label both the stem cell itself and its progeny, bypassing the requirement for "retrospective tracing." Lastly, MADM-based lineage studies allow visualization of axonal and dendritic projections of all progeny, as exemplified from our study of cerebellar granule cells.

MADM Reveals the Relationship between Lineage and Wiring Pattern of Cerebellar Granule Cells

Using the MADM system, we made the unexpected finding that lineage plays a role in directing the axonal projection pattern of cerebellar granule cells (Figure 7F). Postmitotic granule cells are born during the first 3 weeks of postnatal life. However, at E14.5 or before, each granule cell progenitor is already fated to give rise to progeny that project their axons to either (1) a *specific* sublayer of the molecular layer of defined depth or (2) a restricted sublayer, with the specific depth of the sublayer each lineage adopts being a stochastic choice or imposed by later instructions.

Given the relationship between cell cycle exit of granule cells and their axonal projections (see Results), the most plausible explanation for our findings is that clonally related granule cells differentiate within a relatively narrow temporal window. We speculate that this "timed" differentiation could be regulated by extrinsic cues: clonally related granule cells could be made genetically different (e.g., by inheriting different lineage factors) so that each is responsive to a unique combination of extrinsic factors that signals cells to exit the cell cycle. It could also be achieved through an intrinsic "time clock" mechanism as has been described in the differentiation of oligodendrocyte progenitors in vitro: sister cells exit mitosis after the same number of divisions, as if they possess a cell-division-counting device (Temple and Raff, 1986). We are currently investigating these possible mechanisms.

Further Development of the MADM System for Wider Applications

Now that Cre-loxP has been shown to efficiently mediate recombination between homologous chromosomes in mouse somatic cells, we envision further development based on the MADM strategy for wider applications. First, newer versions of RFP that have brighter fluorescence and better stability (Vintersten et al., 2004; Shaner et al., 2004) can be used to replace Dsred2 so that both red and green fluorescence can be visualized in live animals. This will allow genotyping of cells in live animals, which facilitates development, physiology, and imaging experiments to analyze mutant phenotypes.

Second, the split marker gene can be replaced with a split transcription factor that can drive binary expression in the mouse, such as the GAL4/UAS (Ornitz et al., 1991; Rowitch et al., 1999) or the tetracycline-regulatory system (Gossen and Bujard, 1992). In this way, MADM can be used to delete genes as well as to overexpress wild-type or mutant transgenes in small populations of cells for gain-of-function experiments. Indeed, simultaneous loss- and gain-of-function experiments can be performed in the same animal for the same population of labeled cells, as has been done with *Drosophila* MARCM (e.g., Komiyama et al., 2003). With a split transcription factor for binary expression, one can also more easily build other reporters, such as genetically encoded Ca^{2+} or voltage sensors to measure neural activity in a defined population of neurons.

Third, systematic establishment of MADM knockins on all chromosomes will overcome the current limitation of analyzing genes distal to *ROSA26* on chromosome 6. It should be possible to identify chromosomal loci that tolerate homozygous insertion and permit gene expression from the pCA promoter, as in the case of *ROSA26*. A likely complication is the finding that the frequencies of mitotic recombination in ES cells vary according to different loci (Liu et al., 2002). Although it will be labor intensive to generate these mice, once established they will facilitate conditional knockout of individual genes without creating a floxed allele for each gene. In addition, MADM can be used for mosaic forward genetic screens analogous to what has been done in *Drosophila* (Xu and Rubin, 1993), especially if phenotypes can be scored without sacrificing the genetically mosaic animal. This approach can be used, for instance, to identify tumor suppressor genes by looking for tumors in external tissues using specific Cre lines (such as K5-Cre for epidermal tissue) to generate genetic mosaics. Thus, MADM-mediated conditional knockouts of tumor suppressor genes could serve as excellent animal models of human cancers, as MADM can create sparse loss-of-heterozygosity events to follow tumor progression in live animals.

In summary, we expect that the MADM system described in this study and its further development outlined above will be a useful tool to study a plethora of problems in neurobiology, developmental biology, and cancer biology.

Experimental Procedures

Generation of Targeting Constructs

The chimeric MADM targeting constructs (Figure 2A) used mut4-EGFP (Okada et al., 1999) and Dsred2 (Clontech, Palo Alto, Cali-

fornia) tagged with six copies of the MYC epitope at its C terminus. After choosing the break points in the coding sequences, a loxP site-containing β-globin intron (provided by X.-D. Fu of the University of California, San Diego) was inserted through a four step cloning strategy: (1) the 5′ end of the intron followed by a BglII site was fused to the end of N-terminal coding sequence by PCR; (2) the remaining part of the intron led by BglII-loxP was fused to a small front portion of C-terminal part of the coding sequence; (3) the remaining part of C-terminal coding sequence was generated by PCR; (4) all three DNA fragments were ligated into the final products N-GFP (or Dsred2)—5′-intron-BglII-loxP-intron-3′—C-GFP (or Dsred2). The BglII site served as the swapping point between GFP and Dsred2 to generate the chimeric GR and RG constructs as well as the insertion site for *Neo*^{r} preceded by another loxP site. The two chimeric constructs and a third positive control construct, N-GFP—loxP-containing intron—C-GFP (Figure 2A), were inserted into an expression vector (pCA-HZ2) containing a CMV β-actin enhancer-promoter (Okada et al., 1999) and a SV40 T antigen poly(A) signal. The final targeting vectors are constructed by inserting the entire chimeric or control cassettes (from the promoter to the poly(A) signal) into the pROSA26-PA targeting vector (Srinivas et al., 2001) by PacI and AscI.

Biolistic Transfection of Hippocampal Slices

Hippocampal slices were prepared from P7 Long Evans rats as previously described (Nakayama et al., 2000). After 48 hr culture, 1.6 μm gold beads coated with plasmids were propelled into hippocampal slices with a helium burst of 160 pounds per square inch (psi) using the Gene Gun (Bio-Rad). Forty-eight hours after transfection, slices were fixed for immunofluorescence (see Nakayama et al., 2000).

Generating the MADM Mice by Knockin

The ES cell transfection was performed by the Stanford transgenic facility using an R1 cell line. The targeting constructs were linearized by KpnI prior to electroporation. After 125 μg/ml G418 selection, positive clones were identified by two sets of PCR (Figure 2A). Rosa3 (5′-CCACTGACCGCACGGGGATTC-3′) and Rosa4 (5′-TCAATGGGCGGGGGTCGTT-3′) generate a 1.5 kb band with proper recombination of the 5′ arm, while Rosa8 (5′-GAATTCTAG ATAACTGATCATAATCAGCC-3′) and Rosa9 (5′-GGGGAAAATTTT TAATATAAC-3′) generate a 5.7 kb band with proper recombination of the 3′ arm. Two clones of each construct were injected into a C57BL/6 blastocyst to produce chimeric mice. Germline transmission was confirmed by PCR designed to discriminate wt from knockin alleles for all three lines. Rosa10 in 5′ arm forward direction (5′-CTCTGCTGCCTCCTGGCTTCT-3′) and Rosa11 in 3′ arm reverse direction (5′-CGAGGCGGATCACAAGCAATA-3′) amplify a 330 bp fragment from wt alleles, while Rosa10 and Rosa4 in pCA promoter amplify a 250 bp fragment from knockin alleles. PCR conditions: 94°C 20″, 58°C 25″, 72°C 45″ for 32 cycles.

Mating Schemes for MADM Analysis

RG and GR mice were kept as separate stocks prior to MADM analysis. RG mice were crossed with appropriate Cre mice (Table 1), and double positives were selected as stock mice, which were subsequently crossed with GR mice to generate GR/RG;Cre$^+$/+ mice for MADM analysis, and GR/RG;Cre$^-$ mice for controls. The presence of Cre transgene was determined by PCR using specific primers internal to the Cre coding region.

Tissue Preparation and Histology

All animal procedures were based on animal care guidelines and are approved by Stanford University's Administrative Panels on Laboratory Care (A-PLAC). For histology, mice were anesthetized with ketamine/xylazine (60 mg/kg and 8 mg/kg, respectively) and perfused with 4% paraformaldehyde (PFA) in 0.1M phosphate buffer saline (PBS). Tissues were isolated and fixed in 4% PFA at 4°C overnight, washed three times in PBS, cryoprotected for 24 hr in 30% sucrose in PBS, and embedded in OCT prior to cryostat sectioning. Tissues were sectioned at 25 μm thickness unless otherwise specified.

Hematoxylin and eosin staining was performed using standard protocols. For immunofluorescence, cryosections were washed three times for 10 min in PBS, blocked with 10% normal donkey serum in PBS + 0.3% Triton X-100 (PBT) for 20 min, and stained at 4°C overnight with rabbit anti-GFP (1:500; Molecule Probes, Eugene, Oregon) and goat anti-MYC (1:200; Novus, Littleton, Colorado). Following PBT washes, the sections were stained at 4°C overnight with donkey anti-rabbit Alexa 488 (1:100; Molecule Probes, Eugene, Oregon) and donkey anti-goat Cy3 (1:500; Jackson ImmunoResearch Laboratories, Inc. West Grove, Pennsylvania). After further washes with PBT, samples were mounted in anti-fade (Molecular Probes). Images were taken under a Nikon microscope attached to a Bio-Rad MRC-1024 laser scanning confocal system or a Zeiss fluorescence microscope with a CCD camera and processed with the NIH Image J program.

Quantification of Labeling Frequency Using Parallel Fiber Number

Confocal microscopy was used to take 1 μm thick optical sections of the ML from midsagittal sections of the cerebellum from GR/RG;actin-Cre/+ and GR/RG;actin-Cre/actin-Cre. Three images per animal were taken in consecutive 25 μm medial sections at random within the ML in the bank region of lobule 4. Parallel fiber numbers were manually counted as dots in confocal images.

Cell Dissociation and Quantification of Labeling Frequency

Cortical caps of P5 GR/RG;Foxg1/+ mice were enzymatically dissociated as previously described (Machold et al., 2003). Dissociated cells were prepared for immunofluorescence using the Caltag Fix & Perm protocol and placed on a hemocytometer for manual cell quantification using GFP, Cy3 (for MYC staining), and double-channel filters under a fluorescence microscope. FACS analysis (replacing Cy3 with RPE secondary antibodies) using a Coulter Epics XL-MCL FACS Analyzer confirmed the manual counting results.

Clonal Analysis in the Cerebellum

TM (Sigma T-5648) was dissolved in corn oil (Sigma C-8267) at a concentration of 20 mg/ml for ~4 hr at room temperature, stored at 4°C covered with aluminum foil, and used within 2 weeks. To induce interchromosomal recombination in GR/RG;actin-CreER/+ pups, 8–10 mg of TM was administered by intraperitoneal injection of the mother at 13.5 and 17.5 days postcoitum. Controls were given corn oil without TM. Serial sagittal sections of P21 cerebella at 25 or 60 μm were stained and imaged. Mediolateral and anteroposterior span was measured for clones by systematically viewing all serial sections. High-resolution CCD camera images were taken to measure granule cell body position. Confocal microscopy was used to take 1 μm thick images of the ML and to measure granule cell axon position.

To estimate the probability that a cluster of granule cells is derived from two independent but overlapping clones, we estimated the surface area of the IGL for half the cerebellum to be ~197 mm^2 and the surface area occupied by the cell bodies of an average-sized granule cell cluster to be ~0.96 mm^2. To distinguish between two clones, they must not overlap or touch at the edges. Thus, we multiplied the surface area of one average-sized clone by nine to account for the area that a second clone cannot occupy. The probability is: 9 × 0.96 mm^2/197 mm^2 × 100% = 4.4%.

Supplemental Data

Supplemental Data include two figures and can be found with this article online at http://www.cell.com/cgi/content/full/121/3/479/DC1/.

Acknowledgments

We are most grateful to S. McConnell for advice and support. We thank many other Stanford colleagues for advice, in particular B. Barres, G. Barsh, R. Friedel, J. Hebert, and S. Wang. We thank Y. Chen-Tsai and E. Allen for help in generating knockin mice and J. Zhong for technical support, X.-D. Fu and F. Costantini for vectors, and A. Joyner, C. Lobe, J. Mann, G. Martin, S. McConnell, A. McMahon, A. Ramirez, G. Shütz, and W. Zhong for generously providing

Cre lines. We thank G. Jefferis, S. McConnell, S. Narayan, M. Scott, and R. Tsien for comments on this manuscript. J.S.E. is a NDSEG predoctoral fellow. M.D.M. was a recipient of the Stanford Medical Scholars Research Fellowship. This work was supported by a McKnight Technological Innovations in Neuroscience Award to L.L.

Received: December 20, 2004
Revised: January 30, 2005
Accepted: February 10, 2005
Published: May 5, 2005

References

Altman, J., and Bayer, S.A. (1997). Development of the Cerebellar System in Relation to Its Evolution, Structure and Function (New York: CRC Press).

Austin, C.P., Battey, J.F., Bradley, A., Bucan, M., Capecchi, M., Collins, F.S., Dove, W.F., Duyk, G., Dymecki, S., Eppig, J.T., et al. (2004). The knockout mouse project. Nat. Genet. *36*, 921–924.

Badea, T.C., Wang, Y., and Nathans, J. (2003). A noninvasive genetic/pharmacologic strategy for visualizing cell morphology and clonal relationships in the mouse. J. Neurosci. *23*, 2314–2322.

Bonnerot, C., and Nicolas, J.F. (1993). Clonal analysis in the intact mouse embryo by intragenic homologous recombination. C. R. Acad. Sci. III *316*, 1207–1217.

Brakebusch, C., Grose, R., Quondamatteo, F., Ramirez, A., Jorcano, J.L., Pirro, A., Svensson, M., Herken, R., Sasaki, T., Timpl, R., et al. (2000). Skin and hair follicle integrity is crucially dependent on beta 1 integrin expression on keratinocytes. EMBO J. *19*, 3990–4003.

Buffelli, M., Burgess, R.W., Feng, G., Lobe, C.G., Lichtman, J.W., and Sanes, J.R. (2003). Genetic evidence that relative synaptic efficacy biases the outcome of synaptic competition. Nature *424*, 430–434.

Cajal, S.R. (1911). Histology of the Nervous System of Man and Vertebrates (Oxford: Oxford University Press, Inc.).

Cepko, C.L., Ryder, E.F., Austin, C.P., Walsh, C., and Fekete, D.M. (1993). Lineage analysis using retrovirus vectors. Methods Enzymol. *225*, 933–960.

Danielian, P.S., Muccino, D., Rowitch, D.H., Michael, S.K., and McMahon, A.P. (1998). Modification of gene activity in mouse embryos in utero by a tamoxifen-inducible form of Cre recombinase. Curr. Biol. *8*, 1323–1326.

De Paola, V., Arber, S., and Caroni, P. (2003). AMPA receptors regulate dynamic equilibrium of presynaptic terminals in mature hippocampal networks. Nat. Neurosci. *6*, 491–500.

Feil, R., Brocard, J., Mascrez, B., LeMeur, M., Metzger, D., and Chambon, P. (1996). Ligand-activated site-specific recombination in mice. Proc. Natl. Acad. Sci. USA *93*, 10887–10890.

Feng, G., Mellor, R.H., Bernstein, M., Keller-Peck, C., Nguyen, Q.T., Wallace, M., Nerbonne, J.M., Lichtman, J.W., and Sanes, J.R. (2000). Imaging neuronal subsets in transgenic mice expressing multiple spectral variants of GFP. Neuron *28*, 41–51.

Golic, K.G., and Lindquist, S. (1989). The FLP recombinase of yeast catalyzes site-specific recombination in the *Drosophila* genome. Cell *59*, 499–509.

Gong, S., Zheng, C., Doughty, M.L., Losos, K., Didkovsky, N., Schambra, U.B., Nowak, N.J., Joyner, A., Leblanc, G., Hatten, M.E., and Heintz, N. (2003). A gene expression atlas of the central nervous system based on bacterial artificial chromosomes. Nature *425*, 917–925.

Gossen, M., and Bujard, H. (1992). Tight control of gene expression in mammalian cells by tetracycline-responsive promoters. Proc. Natl. Acad. Sci. USA *89*, 5547–5551.

Grueber, W.B., Jan, L.Y., and Jan, Y.N. (2002). Tiling of the *Drosophila* epidermis by multidendritic sensory neurons. Development *129*, 2867–2878.

Gu, H., Marth, J.D., Orban, P.C., Mossmann, H., and Rajewsky, K. (1994). Deletion of a DNA polymerase beta gene segment in T cells using cell type-specific gene targeting. Science *265*, 103–106.

Guo, C., Yang, W., and Lobe, C.G. (2002). A Cre recombinase transgene with mosaic, widespread tamoxifen-inducible action. Genesis *32*, 8–18.

Hallonet, M.E., and Le Douarin, N.M. (1993). Tracing neuroepithelial cells of the mesencephalic and metencephalic alar plates during cerebellar ontogeny in quail-chick chimaeras. Eur. J. Neurosci. *5*, 1145–1155.

Hashimoto, M., and Mikoshiba, K. (2004). Neuronal birthdate-specific gene transfer with adenoviral vectors. J. Neurosci. *24*, 286–296.

Hatten, M.E., and Heintz, N. (1995). Mechanisms of neural patterning and specification in the developing cerebellum. Annu. Rev. Neurosci. *18*, 385–408.

Hayashi, S., and McMahon, A.P. (2002). Efficient recombination in diverse tissues by a tamoxifen-inducible form of Cre: a tool for temporally regulated gene activation/inactivation in the mouse. Dev. Biol. *244*, 305–318.

Hebert, J.M., and McConnell, S.K. (2000). Targeting of cre to the Foxg1 (BF-1) locus mediates loxP recombination in the telencephalon and other developing head structures. Dev. Biol. *222*, 296–306.

Jefferis, G.S.X.E., Marin, E.C., Stocker, R.F., and Luo, L. (2001). Target neuron prespecification in the olfactory map of *Drosophila*. Nature *414*, 204–208.

Kimmel, R.A., Turnbull, D.H., Blanquet, V., Wurst, W., Loomis, C.A., and Joyner, A.L. (2000). Two lineage boundaries coordinate vertebrate apical ectodermal ridge formation. Genes Dev *14*, 1377–1389.

Knudson, A.G., Jr. (1971). Mutation and cancer: statistical study of retinoblastoma. Proc. Natl. Acad. Sci. USA *68*, 820–823.

Koike, H., Horie, K., Fukuyama, H., Kondoh, G., Nagata, S., and Takeda, J. (2002). Efficient biallelic mutagenesis with Cre/loxP-mediated inter-chromosomal recombination. EMBO Rep. *3*, 433–437.

Komiyama, T., Johnson, W.A., Luo, L., and Jefferis, G.S. (2003). From lineage to wiring specificity: POU domain transcription factors control precise connections of *Drosophila* olfactory projection neurons. Cell *112*, 157–167.

Lee, T., and Luo, L. (1999). Mosaic analysis with a repressible cell marker for studies of gene function in neuronal morphogenesis. Neuron *22*, 451–461.

Lee, T., Lee, A., and Luo, L. (1999). Development of the *Drosophila* mushroom bodies: sequential generation of three distinct types of neurons from a neuroblast. Development *126*, 4065–4076.

Lee, C.H., Herman, T., Clandinin, T.R., Lee, R., and Zipursky, S.L. (2001). N-cadherin regulates target specificity in the *Drosophila* visual system. Neuron *30*, 437–450.

Lendahl, U., Zimmerman, L.B., and McKay, R.D. (1990). CNS stem cells express a new class of intermediate filament protein. Cell *60*, 585–595.

Lewandoski, M. (2001). Conditional control of gene expression in the mouse. Nat. Rev. Genet. *2*, 743–755.

Lewandoski, M., Meyers, E.N., and Martin, G.R. (1997). Analysis of Fgf8 gene function in vertebrate development. Cold Spring Harb. Symp. Quant. Biol. *62*, 159–168.

Liu, P., Jenkins, N.A., and Copeland, N.G. (2002). Efficient Cre-loxP-induced mitotic recombination in mouse embryonic stem cells. Nat. Genet. *30*, 66–72.

Machold, R., Hayashi, S., Rutlin, M., Muzumdar, M.D., Nery, S., Corbin, J.G., Gritli-Linde, A., Dellovade, T., Porter, J.A., Rubin, L.L., et al. (2003). Sonic hedgehog is required for progenitor cell maintenance in telencephalic stem cell niches. Neuron *39*, 937–950.

Marin, E.C., Jefferis, G.S.X.E., Komiyama, T., Zhu, H., and Luo, L. (2002). Representation of the glomerular olfactory map in the *Drosophila* brain. Cell *109*, 243–255.

McConnell, S.K. (1988). Fates of visual cortical neurons in the ferret after isochronic and heterochronic transplantation. J. Neurosci. *8*, 945–974.

Metz, C.W. (1916). Chromosome studies on the *Diptera* II: the paired association of chromosomes in the *Diptera*, and its significance. J. Exp. Zool. *21*, 213–279.

Nakayama, A.Y., Harms, M.B., and Luo, L. (2000). Small GTPases Rac and Rho in the maintenance of dendritic spines and branches in hippocampal pyramidal neurons. J. Neurosci. *20*, 5329–5338.

Niwa, H., Yamamura, K., and Miyazaki, J. (1991). Efficient selection for high-expression transfectants with a novel eukaryotic vector. Gene *108*, 193–200.

Okada, A., Lansford, R., Weimann, J.M., Fraser, S.E., and McConnell, S.K. (1999). Imaging cells in the developing nervous system with retrovirus expressing modified green fluorescent protein. Exp. Neurol. *156*, 394–406.

Ornitz, D.M., Moreadith, R.W., and Leder, P. (1991). Binary system for regulating transgene expression in mice: targeting int-2 gene expression with yeast GAL4/UAS control elements. Proc. Natl. Acad. Sci. USA *88*, 698–702.

Pagliarini, R.A., and Xu, T. (2003). A genetic screen in *Drosophila* for metastatic behavior. Science *302*, 1227–1231.

Petersen, P.H., Zou, K., Hwang, J.K., Jan, Y.N., and Zhong, W. (2002). Progenitor cell maintenance requires numb and numblike during mouse neurogenesis. Nature *419*, 929–934.

Ramirez-Solis, R., Liu, P., and Bradley, A. (1995). Chromosome engineering in mice. Nature *378*, 720–724.

Rodriguez, C.I., and Dymecki, S.M. (2000). Origin of the precerebellar system. Neuron *27*, 475–486.

Rowitch, D.H., S-Jacques, B., Lee, S.M., Flax, J.D., Snyder, E.Y., and McMahon, A.P. (1999). Sonic hedgehog regulates proliferation and inhibits differentiation of CNS precursor cells. J. Neurosci. *19*, 8954–8965.

Ryder, E.F., and Cepko, C.L. (1994). Migration patterns of clonally related granule cells and their progenitors in the developing chick cerebellum. Neuron *12*, 1011–1028.

Sanes, J.R. (1989). Analysing cell lineage with a recombinant retrovirus. Trends Neurosci. *12*, 21–28.

Schnütgen, F., Doerflinger, N., Calleja, C., Wendling, O., Chambon, P., and Ghyselinck, N.B. (2003). A directional strategy for monitoring Cre-mediated recombination at the cellular level in the mouse. Nat. Biotechnol. *21*, 562–565.

Shaner, N.C., Campbell, R.E., Steinbach, P.A., Giepmans, B.N., Palmer, A.E., and Tsien, R.Y. (2004). Improved monomeric red, orange and yellow fluorescent proteins derived from Discosoma sp. red fluorescent protein. Nat. Biotechnol. *22*, 1567–1572.

Smith, A.J., De Sousa, M.A., Kwabi-Addo, B., Heppell-Parton, A., Impey, H., and Rabbitts, P. (1995). A site-directed chromosomal translocation induced in embryonic stem cells by Cre-loxP recombination. Nat. Genet. *9*, 376–385.

Soriano, P. (1999). Generalized lacZ expression with the ROSA26 Cre reporter strain. Nat. Genet. *21*, 70–71.

Srinivas, S., Watanabe, T., Lin, C.S., William, C.M., Tanabe, Y., Jessell, T.M., and Costantini, F. (2001). Cre reporter strains produced by targeted insertion of EYFP and ECFP into the ROSA26 locus. BMC Dev. Biol. *1*, 4.

Tang, S.H., Silva, F.J., Tsark, W.M., and Mann, J.R. (2002). A Cre/loxP-deleter transgenic line in mouse strain 129S1/SvImJ. Genesis *32*, 199–202.

Temple, S., and Raff, M.C. (1986). Clonal analysis of oligodendrocyte development in culture: Evidence for a developmental clock that counts cell divisions. Cell *44*, 773–779.

Tronche, F., Kellendonk, C., Kretz, O., Gass, P., Anlag, K., Orban, P.C., Bock, R., Klein, R., and Schutz, G. (2000). Disruption of the glucocorticoid receptor gene in the nervous system results in reduced anxiety. Nat. Genet. *23*, 99–103.

Van Deursen, J., Fornerod, M., Van Rees, B., and Grosveld, G. (1995). Cre-mediated site-specific translocation between nonhomologous mouse chromosomes. Proc. Natl. Acad. Sci. USA *92*, 7376–7380.

Vintersten, K., Monetti, C., Gertsenstein, M., Zhang, P., Laszlo, L., Biechele, S., and Nagy, A. (2004). Mouse in red: red fluorescent protein expression in mouse ES cells, embryos, and adult animals. Genesis *40*, 241–246.

Wingate, R.J., and Hatten, M.E. (1999). The role of the rhombic lip in avian cerebellum development. Development *126*, 4395–4404.

Xu, T., and Rubin, G.M. (1993). Analysis of genetic mosaics in developing and adult *Drosophila* tissues. Development *117*, 1223–1237.

Zambrowicz, B.P., Imamoto, A., Fiering, S., Herzenberg, L.A., Kerr, W.G., and Soriano, P. (1997). Disruption of overlapping transcripts in the ROSA beta geo 26 gene trap strain leads to widespread expression of beta-galactosidase in mouse embryos and hematopoietic cells. Proc. Natl. Acad. Sci. USA *94*, 3789–3794.

Zheng, B., Sage, M., Sheppeard, E.A., Jurecic, V., and Bradley, A. (2000). Engineering mouse chromosomes with Cre-loxP: range, efficiency, and somatic applications. Mol. Cell. Biol. *20*, 648–655.

Zinyk, D.L., Mercer, E.H., Harris, E., Anderson, D.J., and Joyner, A.L. (1998). Fate mapping of the mouse midbrain-hindbrain constriction using a site-specific recombination system. Curr. Biol. *8*, 665–668.

Zirlinger, M., Lo, L., McMahon, J., McMahon, A.P., and Anderson, D.J. (2002). Transient expression of the bHLH factor neurogenin-2 marks a subpopulation of neural crest cells biased for a sensory but not a neuronal fate. Proc. Natl. Acad. Sci. USA *99*, 8084–8089.

Zugates, C.T., and Lee, T. (2004). Genetic mosaic analysis in the nervous system. Curr. Opin. Neurobiol. *14*, 647–653.